HHS Public Access

Author manuscript

Oncogene. Author manuscript; available in PMC 2024 March 01.

Published in final edited form as:

Oncogene. 2023 March ; 42(11): 848–857. doi:10.1038/s41388-023-02599-5.

E-cadherin is a biomarker for ferroptosis sensitivity in diffuse gastric cancer

Alexander M. Minikes[1], **Yu Song**[1,2,*], **Yan Feng**[1], **Changwhan Yoon**[3,4], **Sam S. Yoon**[3,4], **Xuejun Jiang**[1,*]

[1] -Cell Biology Program, Memorial Sloan Kettering Cancer Center, New York, NY 10065

[2] -Soochow University, Affiliated Zhangjiagang Hospital Department of Oncology, China

[3] -Department of Surgery, Memorial Sloan Kettering Cancer Center, New York, NY 10065

[4] -Department of Surgery, Columbia University Irving Medical Center, New York, NY 10032

Abstract

Gastric cancer is the third most common cause of cancer-related death worldwide. Diffuse type gastric cancer (DGC) is a particularly aggressive subtype that is both difficult to detect and treat. DGC is distinguished by weak cell-cell cohesion, most often due to loss of the cell adhesion protein E-cadherin, a common occurrence in highly invasive, metastatic cancer cells. In this study, we demonstrate that loss-of-function mutation of E-cadherin in DGC cells results in their increased sensitivity to the non-apoptotic, iron-dependent form of cell death, ferroptosis. Homophilic contacts between E-cadherin molecules on adjacent cells suppress ferroptosis through activation of the Hippo pathway. Furthermore, single nucleotide mutations observed in DGC patients that ablate the homophilic binding capacity of E-cadherin reverse the ability of E-cadherin to suppress ferroptosis in both cell culture and xenograft models. Importantly, although E-cadherin loss in cancer cells is considered an essential event for epithelial-mesenchymal transition (EMT) and subsequent metastasis, we found that circulating DGC cells lacking E-cadherin expression possess lower metastatic ability, due to their increased susceptibility to ferroptosis. Together, this study suggests that E-cadherin is a biomarker predicting the sensitivity to ferroptosis of DGC cells, both in primary tumor tissue and in circulation, thus guiding the usage of future ferroptosis-inducing therapeutics for the treatment of DGC.

Introduction

Gastric cancer (GC) is the third most common cause of cancer-related mortality and fifth most common type of cancer worldwide[1]. While rates of the most common Lauren

* -corresponding authors, Yu Song (sy5449@163.com) and Xuejun Jiang (jiangx@mskcc.org).

Contributions:

A.M.M., Y.S., and X.J. conceived and designed the study. A.M.M. performed most of the experiments, with contributions from Y.S. and C.Y. C.Y. and S.S.Y. contributed materials and advice. A.M.M., Y.S., and X.J. performed data analysis and wrote the manuscript. All authors contributed to the writing and editing of the manuscript.

Conflict of interest statement:

X.J. and A.M.M. are inventors of patents relevant to ferroptosis and autophagy. X.J. is a consultant and equity holder of Exarta Therapeutics and Lime Therapeutics.

histological subtype, intestinal type GC, have been declining steadily, frequency of the second most common subtype, diffuse type, is rising and currently accounts for roughly 30% of all GC cases[2, 3]. Diffuse type gastric carcinoma (DGC) is a poorly differentiated carcinoma that grows along the lining of the stomach[3]. While the intestinal GC is associated with risk factors such as diet, cigarette use, and chronic gastritis caused by *H. pylori* infection, DGC is associated with mutations to genes involved in cell-cell adhesion, primarily *CDH1*, encoding the adherens junction protein E-cadherin. Germline mutations to *CDH1* have been shown to cause a heritable predisposition to DGC[3–6]. The association between DGC risk and *CDH1* mutation are so significant that prophylactic gastrectomy is often recommended for family members of DGC patients who harbor mutations to E-cadherin[7–9].

Weak cohesion is a hallmark of DGC, resulting in diffuse tumors along the gastric lining. As a result, DGC is difficult to detect, and is typically found in late stages. The difficulty of early DGC detection renders treatment difficult, as many patients have relatively advanced stages of the diseased by the time of diagnosis. As such, a total gastrectomy with lymphadenectomy is typically required as a curative intervention. Neoadjuvant therapy has also been shown to improve patient outcomes, typically including a combination of 5-fluorouracil and a platinum-based therapy such as cisplatin, improving median survival from 27 months after surgery alone to 36 months[10].

Loss of E-cadherin-mediated adhesion is a primary risk factor in DGC. E-cadherin, or cadherin 1, is a member of the cadherin family of proteins which participates in homophilic binding with cadherin molecules on adjacent cells, forming the core of adherens junctions[11]. E-cadherin is a transmembrane protein, with an intracellular domain that binds the other proteins that comprise adherens junctions, the catenins. β-catenin and p120 catenin bind directly with each other, while α-catenin binds both β-catenin and the actin cytoskeleton, linking E-cadherin to the regulation of mechanical forces on the cell[12]. The extracellular domain of E-cadherin is composed of five extracellular cadherin (EC) repeat domains, numbered EC1 at the N-terminus to EC5, ending at the plasma membrane. The exact mechanism of how E-cadherin homophilic binding occurs remains unclear, though the “linear zipper” model, while modified over time, has lasted in the field[11, 13, 14]. Within the EC1 domain, a hydrophobic pocket is formed by K179, D181, and E243 residues which can fit W156 (the second position in the mature protein)[15]. This binding site has been proposed to be involved in binding in *trans* (binding E-cadherin on another cell)[16]. A second binding domain exists on the opposite side of the protein chain between EC1 and EC2, which most likely facilitates binding in *cis* (E-cadherin molecules on the same cell)[16]. Binding in *cis* appears to enhance the adhesive strength of adherens junctions by aggregating E-cadherin molecules[17]. However, these mechanisms are still under debate in the field[11].

We recently found that loss of E-cadherin enhances sensitivity to ferroptosis, a necrotic cell death modality driven by iron-dependent lipid peroxidation[18]. Mechanistically, loss of E-cadherin inhibits the activity of the tumor suppressive Hippo pathway[19]. The Hippo pathway is a central mediator of contact inhibition of cell growth, stopping cells from growing when they contact other cells, in an E-cadherin-dependent manner[18–20].

E-cadherin-mediated cell-cell adhesion suppresses ferroptotic cell death, which was reversed by inhibiting the homophilic adhesion of E-cadherin molecules on adjacent cells. We also found that other cadherin family members may share this ability; *CDH2*, or N-cadherin-mediated contacts could also suppress ferroptosis[18], though the mutation of other cadherin proteins have not been implicated in cancer. As loss-of-function mutation of E-cadherin is a frequent event in DGC, in this study we investigate the role of E-cadherin in regulating ferroptosis in DGC cells, as well as the underlying mechanism and therapeutic implications. Through a series of cellular and xenograft experiments, we demonstrate that E-cadherin mutation renders DGC cells more sensitive to ferroptosis induction, and this process is mediated by tumor suppressor NF2 and downstream transcription coactivator YAP/TAZ. The therapeutic relevance of ferroptosis induction is further supported by our observation that ferroptosis inhibition promoted metastasis of DGC cells harboring mutations to *CDH1*.

Results

E-cadherin mediates cell density-regulated ferroptosis in DGC cells

E-cadherin has been shown to suppress ferroptosis through mediating cell-cell contacts in a cell density-dependent manner[18]. To determine whether E-cadherin also mediates cell density-dependent regulation of ferroptosis in gastric cancer cells, we analyzed two DGC cell lines with different expression patterns of E-cadherin (Fig. 1a, b). SNU16 cells cluster via E-cadherin mediated contacts despite being weakly adherent to tissue culture dishes. When cultured at a low density, these cells were sensitive to the GPX4 inhibitor 1S,3R-RSL3 (RSL3), but ferroptosis was suppressed at higher densities (Fig. 1c, d). Similar results were observed using two other ferroptosis inducers, system x_c^- inhibitor erastin2 and cystine starvation (Fig. S1a, b). SNU668 cells suppress E-cadherin via promoter methylation[21]. These cells were sensitive to ferroptosis regardless of cell density (Fig. 1e, f and Fig. S1c, d). Lipid peroxidation and reactive oxygen species (ROS) were suppressed in dense SNU16 cells, but not dense SNU668 cells (Fig. 1g and Fig. S1e). According to DepMap (https://depmap.org/portal/), expression of *CDH1* inversely correlates with cellular dependence on GPX4 among gastric cancer cell lines (Fig. S1f), consistent with our finding that cells with lower or no E-cadherin expression have a stronger reliance on GPX4, a potent ferroptosis suppressor. To further test this potential causative relationship, we generated a CRISPR-Cas9-mediated knockout cell line of E-cadherin in SNU16 cells (Fig. 2a). SNU16 cells lacking E-cadherin (SNU16 sg*CDH1*) were sensitive to ferroptosis when cultured even at high density (Fig. 2B). We also reconstituted E-cadherin into SNU668 cells (Fig. 2c). Dense SNU668 cells expressing E-cadherin had a suppressed response to RSL3 (Fig. 2d). As expected, when the same cells were cultured into 3D tumor spheroids, the spheroids expressing E-cadherin were more resistant to RSL3 (Fig. 2e, f).

Patient-derived E-cadherin missense mutations in ferroptosis regulation

Having confirmed that E-cadherin can regulate ferroptosis in DGC cell lines, we next sought to understand how this process could be impacted by E-cadherin mutations observed in DGC patients. E-cadherin mutation is correlated with poor prognosis of DGC patients, whereas this effect is not apparent in breast lobular carcinoma, another type of cancer with a high frequency of E-cadherin mutations (Fig. S2a, b). A majority of mutations in DGC

patients cause aberrant large deletions or frameshifts to the coding sequence, which would universally result in a loss of function[18]. Selecting point missense mutations has the potential to uncover an interesting mechanism wherein certain functions of E-cadherin such as adhesion or catenin-binding may be intact but its ability to suppress ferroptosis is ablated. Therefore, we generated a cohort of patient-derived missense mutants of E-cadherin by site-directed mutagenesis (Fig. S2c). The first two domains (EC1 and EC2) have been shown to be particularly important for binding[11]. After stably expressing these mutant constructs in SNU16 sg*CDH1* cells and SNU668 cells (defective of endogenous E-cadherin expression), we found that several mutations to EC1 domain (E254Y, D291N) led to decreased stability and cleavage in SNU668 cells, suggesting certain missense mutants observed in patients may lead to loss of function of E-cadherin through protein degradation. However, such degradation appears to be context-dependent as we only observed it in SNU668 cells but not SNU16 sg*CDH1* cells.

We expressed wild type E-cadherin and the four mutant constructs in SNU16 sg*CDH1* cells (cleavage of the E254Y mutant was less apparent in these cells than in SNU668 cells) (Fig. 3a). Cell death was strongly suppressed by wild type E-cadherin. Of the four mutants tested, three were unable to suppress ferroptosis whereas the other one, A634V, located adjacent to the plasma membrane, suppressed ferroptosis as potently as the wild type E-cadherin (Fig. 3b). As the first two cadherin domains are proposed to be the most critical for binding, a mutation to the fifth may not have a critical effect on the homophilic binding activity of E-cadherin. Similar results were observed in SNU668 cells (Fig. 3c, d) and tumor spheroids generated from SNU668 cells (Fig. 3e).

To understand how these mutations might impact ferroptosis, we characterized the effect of these mutations on a series of documented cellular or biochemical activities of E-cadherin. First, none of these mutations affected the proliferation rate of cells (Fig. S3a). All mutants were able to, at least partially, correctly localize to the plasma membrane in SNU668 cells; and we noted the E254Y and R732Q mutants appeared to partially disrupt localization (Fig. S3b) (R732Q is within the transmembrane region). Second, we tested whether these mutants retained the ability to dimerize in *trans*. For this purpose, we subcloned each E-cadherin mutant into expression plasmids containing either a hemagglutinin (HA) or Flag epitope tag at the C-terminus. Cells containing the HA-tagged construct were then cocultured with cells expressing their Flag-tagged counterpart to determine their potential intercellular interaction by Flag immunoprecipitation. While the full length E254Y mutant was not detected in 293T cells likely due to proteolysis, the D291N mutant was less efficient at binding than the wild type or other mutants (Fig. 4a). Thirdly, we employed a wound healing assay to test the effects of E-cadherin mutations on cell motility. As deletions of EC domains enhance cell motility[22], we predicted that the point mutations to the N-terminal cadherin domains would have the greatest effect on the rate of wound healing. The two mutants at the N-terminus, E254Y and D291N, healed a scratch wound as well as the empty vector control, while the others behaved more similarly to the wild type E-cadherin (Fig. 4b and Fig. S3b). For further study, we selected the D291N mutant, due to its clear link between loss of function and ferroptosis, and the A634V mutant, which despite being identified in DGC patients, does not appear to affect E-cadherin activity or ferroptosis sensitivity and effectively serves as a control. Importantly, both mutants colocalized with β-catenin as well

as the wild type (Fig. 4c). A634V, near the end of the extracellular domain, did not affect E-cadherin binding nor the adhesive capability of E-cadherin (Fig. 4a, b). Instead, recent work suggests that this mutation causes altered activity of integrin β1, dysregulating cell-extracellular matrix interactions and enhancing invasiveness without disrupting homophilic binding of E-cadherin[23].

Thus far, we have identified several single nucleotide mutations observed in DGC patients that can reverse cellular sensitivity to ferroptosis as loss of E-cadherin expression. To determine whether these mutations render DGC cells selectively sensitive to ferroptosis induction even under the background of tumor heterogeneity, we cocultured SNU668 cells expressing each of these mutants with SNU668 cells expressing wild type E-cadherin (they were differentially labelled with fluorescence). Indeed, cells expressing a vector control or the D291N mutant were selectively killed off from the mixed population when challenged with RSL3, while cells expressing wild type E-cadherin or the A634V mutant were resistant to RSL3 (Fig. 4c, d). This was not due to a growth disadvantage, as treatment with ferroptosis inhibitor liproxstatin-1 restored the growth of control cells or cells expressing D291N (Fig. 4d).

Hippo pathway and YAP/TAZ-driven transcription mediate E-cadherin-regulated ferroptosis in DGC cells

Previously, we discovered the role of the Hippo pathway and downstream transcription coactivator YAP/TAZ in regulating ferroptosis[18]. As E-cadherin can activate the Hippo pathway, we performed a series of mechanistic experiments linking E-cadherin, the Hippo pathway, and YAP/TAZ in DGC cells. E-cadherin-mediated signals are propagated through cytoskeletal forces to activate the tumor suppressor NF2, also known as merlin[19]. Indeed, hairpins targeting NF2 sensitized SNU16 cells (which express E-cadherin) to ferroptosis (Fig. 5a and Fig. S5a). Further, activity of YAP and TAZ was suppressed in dense SNU16 cells, but not in dense SNU668 cells (which do not express E-cadherin) (Fig. S5b).

We and others identified YAP/TAZ target genes that regulate ferroptosis: *TFRC, ACSL4,* and *NOX4*[18, 24]. Transferrin receptor (TFRC) is responsible for the absorption of transferrin into cells, providing iron, an essential element for the cell but also a catalyst of ferroptosis[25]. Acyl CoA Synthetase Long Chain 4 (ACSL4) promotes the incorporation of oxidation-sensitive long chain polyunsaturated fatty acids into phospholipids, providing substrates for the lipid peroxidation necessary for ferroptosis[26, 27]. The NADPH oxidases (NOXs), including NOX4, produce superoxide as a byproduct of their catalytic activity, and thus inhibition of NOX activity could suppress ferroptosis[28]. Expression of all three of these proteins was suppressed in dense SNU16 cells, but not in dense SNU668 cells (Fig. 5b and Fig. S4c–e). A recent study identified ALOXE3, a member of the arachidonate lipoxygenase family that can directly oxidize arachidonic acids, as another target of YAP and TAZ that regulates ferroptosis[29]. However, we did not observe a significant suppression of ALOXE3 in dense SNU16 cells (Fig. S4f). As expected, expression of the canonical YAP/TAZ targets *CCN1*, also known as CYR61, and *CCN2,* or CTGF, were both strongly suppressed in dense SNU16 cells (Fig. S4g, h).

In both SNU16 sg*CDH1* and SNU668 cells, wild type E-cadherin or A634V could suppress expression of TFRC, ACSL4, and NOX4, whereas D291N failed to do so (Fig. 5c, d). This result supports the mechanism that E-cadherin suppresses ferroptosis via inhibiting YAP/TAZ-driven transcription. Consistent with this mechanism, overexpression of the constitutively active YAP mutant, YAP^{S127A} re-sensitized SNU16 sg*CDH1* cells expressing wild type or A634V E-cadherin to ferroptosis induction (Fig. 5e, S5). Similarly, overexpression of YAP^{S127A} also recovered lipid peroxidation in these cells upon RSL3 treatment (Fig. 5f). Finally, expression of YAP^{S127A} also rendered spheroids sensitive to both RSL3 and erastin, regardless of the status of E-cadherin (Fig. 5g and Fig. S6).

Genetic status of E-cadherin determines metastatic potential of DGC cells and their responsiveness to ferroptosis-inducing therapy

In gastric cancer, mutations to E-cadherin are predictive of poor survival (Fig. S2a). However, we found that cells harboring E-cadherin mutations that disrupt its activity to modulate Hippo-YAP/TAZ signaling are rendered more sensitive to ferroptosis *in vitro*. To test whether E-cadherin mutations may be a biomarker predicting the sensitivity of DGC to ferroptosis-inducing compounds, we generated a subcutaneous xenograft model using SNU16 sg*CDH1* cells expressing a control vector (also recapitulating majority of patient-derived E-cadherin mutation, which is loss of expression), wild type E-cadherin, or the D291N mutant (a patient-derived missense mutation). Firstly, we confirmed that imidazole ketone erastin (IKE), an erastin derivative with improved stability and efficacy in *in vivo* models, could efficiently induce ferroptosis in SNU16 cells defective of *CDH1* expression or expressing inactive mutant of *CDH1* (Fig. S7a). These cells were injected into athymic *nu/nu* mice and tumors were allowed to develop. Once tumors reached a volume of 150 mm^3, mice were administered either a vehicle or imidazole ketone erastin (IKE), an erastin analog that can be used *in vivo*. While cells expressing wild type E-cadherin grew following treatment with IKE, both the vector control and D291N mutant tumors stabilized with treatment (Fig. 6a, b and Fig. S7b). The vector control and D291N tumors both had increased levels of malondialdehyde (MDA), a lipid peroxidation decomposition product used as an indicator of ferroptosis, and a decreased expression of the proliferation marker Ki67 (Fig. 6c). These results indicate that IKE induced ferroptosis to suppress tumor growth. Consistent with our *in vitro* observations, these tumors also had increased nuclear accumulation of YAP and elevated ACSL4 expression (Fig. 6d and Fig. S7c).

A recent study suggested that, paradoxically, while E-cadherin is a suppressor of invasion into the bloodstream, loss of E-cadherin is a liability for circulating tumor cells (CTCs), subjecting them to increased oxidative stress[30]. Therefore, we investigated whether ferroptosis contributes to the vulnerability of circulating gastric cancer cells lacking E-cadherin expression. This is important, as positive result will provide evidence supporting the *in vivo* biological function of ferroptosis in suppressing tumorigenesis, and in this specific case, metastasis associated with loss-of-function mutation of a tumor suppressor. To test this possibility, we injected SNU16 sg*CDH1* expressing a control vector or wild type E-cadherin into the tail vein of mice. Prior to injection, cells were incubated with either ferroptosis inhibitor liproxstatin-1 or DMSO (vehicle control). Four weeks after tail-vein injection, lungs were scanned for metastatic lesions (Fig. 6e, Fig. S7d). While SNU16

sg*CDH1* cells were nearly totally unable to form metastatic lesions, reconstitution of E-cadherin or supplementation with liproxstatin-1 enhanced metastatic colonization following intravenous injection, indicating the role of E-cadherin-mediated ferroptosis suppression in promoting metastasis after intravasation.

Discussion

Treatment options for diffuse gastric cancer (DGC) remain limited. Recently, the FDA and EMA approved the addition of the PD-1 inhibitor nivolumab to the chemotherapy regimen in patients with advanced disease following a clinical study which found a significant improvement in overall survival when adding the immune checkpoint inhibitor to the treatment plan[31]. In advanced GC patients with high tumor expression of PD-L1 (roughly 60% of all patients), median survival improved from 11.1 months to 14.4 months. When all patients were included regardless of PD-L1 expression, survival improved from 11.6 to 13.8 months. While checkpoint inhibitors are a new direction in GC treatment, they only lead to a modest improvement in outcomes, and they may not be suitable for all patients. Therefore, other treatment options should be investigated. Additionally, future studies will be required to understand whether ferroptosis may be a suitable addition to this therapy regimen, which cannot be evaluated using the present xenograft model.

Here we present evidence to support that ferroptosis induction, although still under development and unavailable clinically, may represent a promising therapeutic approach for the treatment of cancers harboring specific oncogenic mutations, e.g., DGC with loss-of-function mutation of E-cadherin, as we demonstrated in both cell culture and mouse xenograft analysis. Whether these therapies may be suitable to use in combination with current first line treatments or as a second line of treatment requires further investigation. Remarkably, mutations of *CDH1* and subsequent activation of YAP/TAZ usually promote malignancy and resistance of cancer cells to common therapies. Therefore, our finding that these same mutations render DGC cells more sensitive to ferroptosis induction indicates the E-cadherin mutations are potential Achilles' heels and biomarkers of DGC guiding the use of ferroptosis-inducing therapies. While several potential biomarkers for ferroptosis sensitivity such as ACSL4[32] or TFRC[33] have been identified, mutation or deletion of E-cadherin in DGC or other cancers is a far more easily evaluable biomarker than making determinations based on gene or protein expression. Further, the highly frequent rate of *CDH1* mutation in various cancers including DGC also makes it a preferred biomarker for predicting responsiveness of these cancers to ferroptosis-inducing therapies.

Mechanistically, this study demonstrated that the adhesive capability of E-cadherin, which is commonly lost in DGC, regulates ferroptosis in both *in vitro* and xenograft models. Both loss of expression and point mutations identified in DGC patients that disrupt the homophilic binding activity of E-cadherin can reverse the effect of E-cadherin on suppressing ferroptosis. Specifically, we found that mutations to residues that interfere with the homophilic binding activity of E-cadherin, either by disrupting localization or binding directly, can block the anti-ferroptotic function of E-cadherin. On the other hand, the A634V mutant, which is predicted to disrupt E-cadherin-extracellular matrix interactions, retains its ability to suppress ferroptosis[23]. Further, we confirmed that these disruptions

to E-cadherin relief the inhibition of YAP/TAZ by the NF2-Hippo pathway, leading to the upregulation of a variety of proteins, including ACSL4, TFRC, NOX4, and ALOXE3. These proteins likely promote a ferroptosis-sensitive state by modifying the phospholipidome and increasing oxidative stress within cells. Interestingly, previous reports also suggest the existence of ferroptosis-sensitive cellular state[34, 35]. For example, epithelial-mesenchymal transition (EMT) and mesenchymal properties have been implicated to define a cellular state more favorable for ferroptosis[35]. The important role of YAP/TAZ in EMT[36] provides a mechanistic explanation for the link between EMT and ferroptosis.

Because of the central role of EMT in metastasis[37], the relationship between EMT and ferroptosis, as well as the role of E-cadherin in both processes, warrants further investigation. Transcriptional suppression of E-cadherin is often associated with EMT[11], presumably facilitating cellular movement through tissue, allowing metastasizing cells to reach distal locations more easily through the body. However, as loss of E-cadherin sensitizes cells to ferroptosis, would metastasizing cells, especially those lacking E-cadherin expression, be more vulnerable to ferroptosis? Our study supports this notion: E-cadherin-expressing DGC cells injected intravenously were able to better colonize and form metastases in the lung than the same cells lacking E-cadherin; conversely, suppression of ferroptosis pharmacologically enhanced metastasis of DGC cells lacking E-cadherin expression. In theory, circulation through the vasculature imparts a great deal of oxidative stress on cells, and ferroptosis may be a consequence of the oxidative stress – this scenario can explain our observation. Similarly, a recent study found that melanoma cells traveling through lymph, which is rich in glutathione and monounsaturated fatty acids (both of which protect against ferroptosis), form metastases better than cells traveling through blood[38]. They also found that suppression of ferroptosis could enhance metastasis of melanoma cells traveling through blood. Furthermore, another study found that loss of E-cadherin can actually make metastasis less efficient once cells reach the bloodstream[39], despite loss of E-cadherin being a central step in EMT. Taken together, it is likely that E-cadherin mutation may impact individual steps of metastasis differentially: it promotes cancer cell intravasation; but once cancer cells reach blood circulation, lack of E-cadherin expression renders these cells more susceptible to oxidative stress and ferroptosis, thus reducing their metastatic potential.

Methods

Cell culture and treatment conditions.

SNU16 and 293T cells were purchased from ATCC. SNU668 cells were obtained from the Korean Cell Line Bank (KCLB). SNU16 and SNU668 cells were cultured in RPMI containing 10% fetal bovine serum (FBS), 100 units ml^{-1} penicillin, and 100 μg ml^{-1} streptomycin (Pen/Strep). 293T cells were cultured in DMEM containing 10% FBS, Pen/Strep, and 2 mM L-glutamine. Cells were kept in an incubator maintained at 37°C and 5% CO_2. Cystine starvation media was prepared as previously described[18]. Erastin2 (Cayman Chemical Company), RSL3, and Lpx-1 (Selleck Chemicals) were all dissolved in DMSO. For experiments, “sparse” is defined as 5×10^3 (SNU16) or 3×10^3 (SNU668) cells in a 96-well and 8×10^4 (SNU16) or 5×10^5 (SNU668) in a 6-well dish. “Dense” is defined

as 5×10^4 (SNU16) or 3×10^4 (SNU668) cells in a 96-well and 8×10^5 (SNU16) or 5×10^5 (SNU668) in a 6-well dish. Cells were grown for 30 hours prior to use for experiments. All cell lines used were sent for STR profiling and routinely monitored for mycoplasma contamination.

Plasmids and cloning.

pGEMT-*CDH1* was purchased from Sino Biological and mutant constructs were generated using the Q5 Site-Directed Mutagenesis kit (New England BioLabs). Primers used for mutagenesis are listed in Supplementary Figure 1. These mutant E-cadherin genes were then subcloned into the pQCXIP backbone. To generate either Flag or HA 3' tags, a fragment was amplified using primers that include the nucleotide sequence for either epitope tag (Supplementary Figure 1). Fragments and each construct were cut with NheI (an internal restriction site) and PacI, gel purified, and ligated together. All constructs were confirmed by sequencing. CRISPR-Cas9-mediated *CDH1* knockout was performed using a pool of three vectors with a single vector containing an sgRNA and Cas9 (Santa Cruz Biotechnology sc-400031). pQCXIH-Flag-YAP-S127A was from Dr. Kunliang Guan's lab (Addgene #33092).

Measurement of cell death.

Cell death was assessed using a high-content imaging assay using a Cytation 5 imaging system. Cells were infected with lentiviruses harboring Histone 2B fused to mCherry (H2B-mCherry, Addgene #20972) in order to label live nuclei. For RSL3 or erastin experiments, cells were imaged in the Cytation 5 equipped with FITC and TexasRed filter sets after 24 hours using a protocol designed in the Gen 5 v3.08 software (BioTek Instruments). For cystine starvation, cells were placed in a BioSpa incubator (BioTek Instruments) linked to the Cytation 5, and cells were imaged every two hours. Four images were taken per well using the 4x objective. Live (SYTOX Green$^-$, SG$^-$) and dead cells (SYTOX Green$^+$, SG$^+$) were identified using a watershedding cell count algorithm using the Gen 5 software. To avoid double counting, double-positive cells (H2B$^+$SG$^+$) were also counted separately. For 24-hour endpoint experiments, cell death was calculated as:

$$cell\ \ death = \ \ 100 \ \ \times \ \ \frac{SG^+}{(SG^+ + SG^- - \ \ H2B^+SG^+)}$$

A similar calculation was used to measure cell death in time course experiments. In order to account for dead cells that detach from the substrate and float away — artificially deflating the SG$^+$ count — we adjusted the SG$^+$ count to use the maximum value between the first image (t = 0) and the current time point *n*, as suggested for the STACK cell death assay[40]:

$$cell\ death_{t=n} = 100 \times \ \ \frac{SG^+_{max_{t=0 \to t=n}}}{(SG^+_{max_{t=0 \to t=n}} + SG^-_{t=n} - \ \ H2B^+SG^+_{t=n})}$$

Immunoblotting.

Protein lysates were collected as previously described[18]. Lysates were separated on 8% gels and transferred to nitrocellulose membranes. Membranes were blocked in 5% skim milk in TBST for one hour. Membranes were incubated overnight at 4°C in primary antibody diluted in TBST and in secondary at room temperature for 1 hour. Blots were imaged using Clarity ECL solution (Bio-Rad) and an Amersham 600 imager (GE Healthcare Life Sciences).

Immunofluorescence.

Cells were prepared as described on glass coverslips. Cells were permeabilized in 0.1% Triton X100 in PBS (*v/v*) and blocked in 1% BSA in PBS (*w/v*). Coverslips were incubated in primary antibodies overnight at 4°C, and secondary antibodies for 30 minutes at room temperature. Widefield microscopy was performed on a Nikon Eclipse Ti-E microscope, with an attached Andor CSU spinning disk confocal microscope for confocal microscopy. Images were captured and analyzed using NIS Elements (Nikon) and Fiji.

Antibodies.

For Western blots, the following antibodies were used: E-cadherin (Abcam, ab76055, 1:1000), β-actin (Sigma-Aldrich A1978, 1:3000); NF2 (Cell Signaling 12888, 1:1000); ACSL4 (Santa Cruz sc-365230, 1:100); TFRC (Abcam ab214039, 1:1000); NOX4 (Abcam ab109225, 1:1000); HA (Sigma-Aldrich H3663, 1:2000); Flag (Sigma-Aldrich F1804, 1:2000); rabbit IgG-HRP (Thermo Fisher 31458, 1:10000); mouse IgG-HRP (Thermo Fisher 31430, 1:10000). For immunofluorescence: E-cadherin (Abcam, ab76055, 1:200); YAP (Cell Signaling 14074, 1:200); HA (Sigma-Aldrich H3663, 1:400); ACSL4 (Thermo Fisher PA5–27137, 1:200); FITC-anti-MDA (ab27615, 1:50); Ki67 (Cell Signaling 9449, 1:400); rabbit IgG-AlexaFluor488 (Invitrogen A11008, 1:500); mouse IgG-AlexaFluor594 (Invitrogen A32744, 1:500).

RT-qPCR.

Cells were washed in PBS and mRNA was collected using TRIzol (Invitrogen) according to the manufacturer's specifications. cDNA was produced using iScript (Bio-Rad) according to the manufacturer's specifications. qPCR was performed using iQ Sybr-Green Master Mix (Bio-Rad) and CFX96 thermocycler (Bio-Rad).

Wound healing assay

8×10^4 SNU668 cells labeled with H2B-mCherry were seeded in 24-well plates (Corning) with a well diameter of 1.6 cm. After 30 hours, cells had reached confluence, and an approximately 200 μm scratch was made down the center of each well using p200 micropipette tip (USA Scientific). Plates were then placed in a Biospa incubator attached to a Cytation 5 imager. Images were taken at two-hour intervals and the rate at which cells closed the 200 μm gap was quantified.

Subcutaneous xenograft models.

7.5×10^6 SNU16 sg*CDH1* cells expressing a vector, wild type E-cadherin, or the D291N mutant in 100 μl 1:1 Matrigel:serum-free RPMI were injected into the left flank of athymic *nu/nu* mice (Envigo). Tumor growth was monitored every three days by caliper. Once tumors reached a mean volume of 150 mm^3, mice with each tumor type were randomly grouped into two groups. IKE (MedChemExpress) was resuspended in a solution of 65% D5W (5% dextrose in water), 5% Tween-80, and 30% PEG-400. Mice were then treated daily with either 40 mg kg^{-1} IKE or the vehicle via i.p. injection.

Mice were euthanized at a pre-determined endpoint using CO_2 and tumors were resected and weighed. According to the Institutional Animal Care and Use Committee (IACUC) protocol for these experiments, once any tumor exceeded a volume of 1,000 mm^3, 1.5 cm in diameter or 10% of body weight, the mice would immediately be euthanized. At the end of the study, mice were euthanized with CO_2 and tumors were taken for immunohistochemical staining. Results are presented as mean tumor volume ± s.d.

All protocols were approved by the Memorial Sloan Kettering Cancer Center IACUC.

Immunohistochemistry.

Excised tumors were weighed and washed in PBS without calcium and magnesium. Tumors were then fixed in 4% fresh formaldehyde at 4°C for roughly 16 hours, followed by immersion in 30% sucrose in PBS (*w/v*) at 4°C, rotating until tumors sank to the bottom of the tube. Tumors were then embedded in OCT (Sakura Finetek) and frozen at −80°C. 10-μm thick sections were made on a cryostat (Leica) set to −20°C and transferred to Superfrost Plus microscope slides (Fisher Scientific). Slides were then washed in PBS to remove the remaining OCT, permeabilized in 0.2% Triton X-100, and blocked in 1% BSA in PBS for 1 hour at room temperature containing 0.1 μg ml^{-1} Hoechst 33342 (Thermo Scientific). Primary antibodies were diluted in blocking buffer and incubated for 2 hours at room temperature. Anti-rabbit or mouse IgG conjugated to AlexaFluor-594 (Invitrogen) was diluted in blocking buffer and incubated for 1 hour at room temperature. Slides were dried, mounted, and imaged by microscopy.

Tail vein metastasis model.

SNU16 sg*CDH1* were infected with lentiviruses to stably express a fluorescent marker, iRFP-720 (Addgene #104587). After flow assisted cell sorting (FACS), cells were engineered to express either a vector control or wild type E-cadherin. These cells were trypsinized, counted, resuspended in serum-free RPMI, and passed through a strainer to obtain a single cell suspension. Cells were then incubated with either DMSO or 2 μM liproxstatin-1 for 30 minutes. Mice were randomly assigned into groups and a heat lamp was used to dilate tail veins briefly. 1×10^6 cells were injected through the tail vein in 100 μL using a 28g needle. Mice were monitored immediately after injection for labored breathing or other signs of stress, and daily thereafter for overall health. After four weeks, mice were euthanized and lungs were excised.

50-μm cryosections were obtained, roughly 12 from each lung. Sections were washed in PBS, counterstained with Hoechst 33342 (Invitrogen), and mounted. Slides were scanned for clusters of 50 or more cells expressing the far-red fluorescent marker iRFP720.

All protocols were approved by the Memorial Sloan Kettering Cancer Center IACUC.

Statistical analysis.

Experiments are the result of at least three biological replicates. Western blots and micrographs are representative images of at least three biological replicates. Statistical analyses were performed using Prism 6.0 (GraphPad). If individual data points are not represented, data are presented as mean ± s.d. from three independent experiments. *P* values were determined Student's t-test or ANOVA with Tukey's multiple comparison test as indicated. *P* values are represented by asterisks: *: $P < 0.05$; **: $P < 0.01$; ***: $P < 0.001$; ****: $P < 0.0001$; *NS*: not significant. Exact *P* values are listed in each corresponding figure legend, referring to asterisks from left to right or (if listed in the key) top to bottom. Unless otherwise stated, experiments were not randomized, and investigators were not blinded.

Supplementary Material

Refer to Web version on PubMed Central for supplementary material.

Acknowledgments:

The authors thank members of the Jiang lab for critical reading and suggestions. This work is supported by NIH F31CA247112 (to A.M.M.), NIH R01CA204232 and NIH R01CA258622 (to X.J.), and NCI cancer centre core grant P30 CA008748 to MSKCC.

Data availability:

All raw data values and Western blots are available as Supplemental Data. All other relevant data is available upon request from the authors.

References

1. Sung H, Ferlay J, Siegel RL, Laversanne M, Soerjomataram I, Jemal A et al. Global Cancer Statistics 2020: GLOBOCAN Estimates of Incidence and Mortality Worldwide for 36 Cancers in 185 Countries. CA: A Cancer Journal for Clinicians 2021; 71: 209–249. [PubMed: 33538338]
2. Crew KD, Neugut AI. Epidemiology of gastric cancer. World J Gastroenterol 2006; 12: 354–362. [PubMed: 16489633]
3. Ansari S, Gantuya B, Tuan VP, Yamaoka Y. Diffuse Gastric Cancer: A Summary of Analogous Contributing Factors for Its Molecular Pathogenicity. Int J Mol Sci 2018; 19.
4. Liu X, Chu K-M. E-cadherin and gastric cancer: cause, consequence, and applications. Biomed Res Int 2014; 2014: 637308. [PubMed: 25184143]
5. Kaurah P, MacMillan A, Boyd N, Senz J, De Luca A, Chun N et al. Founder and Recurrent CDH1 Mutations in Families With Hereditary Diffuse Gastric Cancer. JAMA 2007; 297: 2360–2372. [PubMed: 17545690]
6. Till JE, Yoon C, Kim B-J, Roby K, Addai P, Jonokuchi E et al. Oncogenic KRAS and p53 Loss Drive Gastric Tumorigenesis in Mice That Can Be Attenuated by E-Cadherin Expression. Cancer Research 2017; 77: 5349–5359. [PubMed: 28760854]

7. Lewis FR, Mellinger JD, Hayashi A, Lorelli D, Monaghan KG, Carneiro F et al. Prophylactic total gastrectomy for familial gastric cancer. Surgery 2001; 130: 612–617; discussion 617–619. [PubMed: 11602891]
8. Shenoy S CDH1 (E-Cadherin) Mutation and Gastric Cancer: Genetics, Molecular Mechanisms and Guidelines for Management. Cancer Manag Res 2019; 11: 10477–10486. [PubMed: 31853199]
9. Pandalai PK, Lauwers GY, Chung DC, Patel D, Yoon SS. Prophylactic total gastrectomy for individuals with germline CDH1 mutation. Surgery 2011; 149: 347–355. [PubMed: 20719348]
10. Sitarz R, Skierucha M, Mielko J, Offerhaus GJA, Maciejewski R, Polkowski WP. Gastric cancer: epidemiology, prevention, classification, and treatment. Cancer Manag Res 2018; 10: 239–248. [PubMed: 29445300]
11. van Roy F, Berx G. The cell-cell adhesion molecule E-cadherin. Cell Mol Life Sci 2008; 65: 3756–3788. [PubMed: 18726070]
12. Perez-Moreno M, Fuchs E. Catenins: keeping cells from getting their signals crossed. Developmental cell 2006; 11: 601–612. [PubMed: 17084354]
13. Koch AW, Manzur KL, Shan W. Structure-based models of cadherin-mediated cell adhesion: the evolution continues. Cellular and Molecular Life Sciences 2004; 61: 1884–1895. [PubMed: 15289931]
14. Shapiro L, Fannon AM, Kwong PD, Thompson A, Lehmann MS, Grübel G et al. Structural basis of cell-cell adhesion by cadherins. Nature 1995; 374: 327–337. [PubMed: 7885471]
15. Parisini E, Higgins JM, Liu JH, Brenner MB, Wang JH. The crystal structure of human E-cadherin domains 1 and 2, and comparison with other cadherins in the context of adhesion mechanism. J Mol Biol 2007; 373: 401–411. [PubMed: 17850815]
16. Boggon TJ, Murray J, Chappuis-Flament S, Wong E, Gumbiner BM, Shapiro L. C-Cadherin Ectodomain Structure and Implications for Cell Adhesion Mechanisms. Science 2002; 296: 1308–1313. [PubMed: 11964443]
17. Brieher WM, Yap AS, Gumbiner BM. Lateral dimerization is required for the homophilic binding activity of C-cadherin. J Cell Biol 1996; 135: 487–496. [PubMed: 8896604]
18. Wu J, Minikes AM, Gao M, Bian H, Li Y, Stockwell BR et al. Intercellular interaction dictates cancer cell ferroptosis via NF2-YAP signalling. Nature 2019; 572: 402–406. [PubMed: 31341276]
19. Kim NG, Koh E, Chen X, Gumbiner BM. E-cadherin mediates contact inhibition of proliferation through Hippo signaling-pathway components. Proc Natl Acad Sci U S A 2011; 108: 11930–11935. [PubMed: 21730131]
20. Meng Z, Moroishi T, Guan KL. Mechanisms of Hippo pathway regulation. Genes Dev 2016; 30: 1–17. [PubMed: 26728553]
21. Kim TY, Jong H-S, Jung Y, Kim T-Y, Kang GH, Bang Y-J. DNA hypermethylation in gastric cancer. Alimentary Pharmacology & Therapeutics 2004; 20: 131–142. [PubMed: 15298619]
22. Handschuh G, Candidus S, Luber B, Reich U, Schott C, Oswald S et al. Tumour-associated E-cadherin mutations alter cellular morphology, decrease cellular adhesion and increase cellular motility. Oncogene 1999; 18: 4301–4312. [PubMed: 10439038]
23. Figueiredo J, Ferreira RM, Xu H, Gonçalves M, Barros-Carvalho A, Cravo J et al. Integrin β1 orchestrates the abnormal cell-matrix attachment and invasive behaviour of E-cadherin dysfunctional cells. Gastric Cancer 2022; 25: 124–137. [PubMed: 34486077]
24. Yang WH, Ding CC, Sun T, Rupprecht G, Lin CC, Hsu D et al. The Hippo Pathway Effector TAZ Regulates Ferroptosis in Renal Cell Carcinoma. Cell Rep 2019; 28: 2501–2508.e2504. [PubMed: 31484063]
25. Gao M, Monian P, Quadri N, Ramasamy R, Jiang X. Glutaminolysis and Transferrin Regulate Ferroptosis. Molecular cell 2015; 59: 298–308. [PubMed: 26166707]
26. Kagan VE, Mao G, Qu F, Angeli JP, Doll S, Croix CS et al. Oxidized arachidonic and adrenic PEs navigate cells to ferroptosis. Nat Chem Biol 2017; 13: 81–90. [PubMed: 27842066]
27. Doll S, Proneth B, Tyurina YY, Panzilius E, Kobayashi S, Ingold I et al. ACSL4 dictates ferroptosis sensitivity by shaping cellular lipid composition. Nat Chem Biol 2017; 13: 91–98. [PubMed: 27842070]
28. Dixon SJ, Lemberg KM, Lamprecht MR, Skouta R, Zaitsev EM, Gleason CE et al. Ferroptosis: an iron-dependent form of nonapoptotic cell death. Cell 2012; 149: 1060–1072. [PubMed: 22632970]

29. Qin Y, Pei Z, Feng Z, Lin P, Wang S, Li Y et al. Oncogenic Activation of YAP Signaling Sensitizes Ferroptosis of Hepatocellular Carcinoma via ALOXE3-Mediated Lipid Peroxidation Accumulation. Front Cell Dev Biol 2021; 9: 751593. [PubMed: 34977009]
30. Padmanaban V, Krol I, Suhail Y, Szczerba BM, Aceto N, Bader JS et al. E-cadherin is required for metastasis in multiple models of breast cancer. Nature 2019; 573: 439–444. [PubMed: 31485072]
31. Janjigian YY, Shitara K, Moehler M, Garrido M, Salman P, Shen L et al. First-line nivolumab plus chemotherapy versus chemotherapy alone for advanced gastric, gastro-oesophageal junction, and oesophageal adenocarcinoma (CheckMate 649): a randomised, open-label, phase 3 trial. Lancet 2021; 398: 27–40. [PubMed: 34102137]
32. Yuan H, Li X, Zhang X, Kang R, Tang D. Identification of ACSL4 as a biomarker and contributor of ferroptosis. Biochem Biophys Res Commun 2016; 478: 1338–1343. [PubMed: 27565726]
33. Feng H, Schorpp K, Jin J, Yozwiak CE, Hoffstrom BG, Decker AM et al. Transferrin Receptor Is a Specific Ferroptosis Marker. Cell Rep 2020; 30: 3411–3423 e3417. [PubMed: 32160546]
34. Hangauer MJ, Viswanathan VS, Ryan MJ, Bole D, Eaton JK, Matov A et al. Drug-tolerant persister cancer cells are vulnerable to GPX4 inhibition. Nature 2017; 551: 247–250. [PubMed: 29088702]
35. Viswanathan VS, Ryan MJ, Dhruv HD, Gill S, Eichhoff OM, Seashore-Ludlow B et al. Dependency of a therapy-resistant state of cancer cells on a lipid peroxidase pathway. Nature 2017; 547: 453–457. [PubMed: 28678785]
36. Yamaguchi H, Taouk GM. A Potential Role of YAP/TAZ in the Interplay Between Metastasis and Metabolic Alterations. Frontiers in Oncology (Review) 2020; 10.
37. Heerboth S, Housman G, Leary M, Longacre M, Byler S, Lapinska K et al. EMT and tumor metastasis.
38. Ubellacker JM, Tasdogan A, Ramesh V, Shen B, Mitchell EC, Martin-Sandoval MS et al. Lymph protects metastasizing melanoma cells from ferroptosis. Nature 2020; 585: 113–118. [PubMed: 32814895]
39. Padmanaban V, Krol I, Suhail Y, Szczerba BM, Aceto N, Bader JS et al. E-cadherin is required for metastasis in multiple models of breast cancer2019.
40. Forcina GC, Conlon M, Wells A, Cao JY, Dixon SJ. Systematic Quantification of Population Cell Death Kinetics in Mammalian Cells. Cell Syst 2017; 4: 600–610 e606.

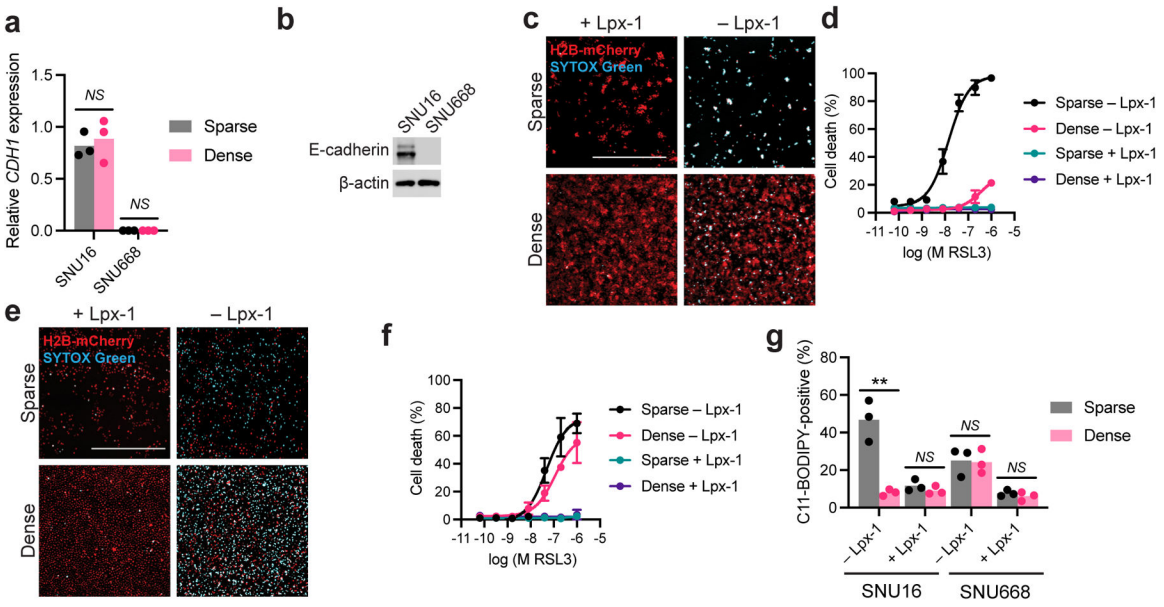

Figure 1. Effect of cell density on ferroptosis of DGC cells.

a, Measurement of *CDH1* expression in SNU16 and SNU668 cells by qPCR after culture at their respective sparse or dense concentrations (see Methods). *P* = 0.6442, 0.2421 (from left to right). **b,** E-cadherin expression was assessed in SNU16 and SNU668 cells. **c-d,** SNU16 cells were cultured either sparse or dense and treated with various concentrations of RSL3 for 24 hours with or without 1 μM liproxstatin-1 (Lpx-1). **c,** Representative images of cells treated with 1 μM RSL3 collected by Cytation 5 imaging. **d,** Data after image analysis by Gen5 software. **e-f**, SNU668 cells were treated and analyzed as described in **c** and **d.** **g,** SNU16 and SNU668 cells were treated with 0.5 μM RSL3 for 18 hours, stained with C11-BODIPY for lipid peroxidation quantitation by flow cytometry. *P* = 0.0038, 0.3015, 0.8800, 0.3898. Statistical analysis was performed by student's t-test.

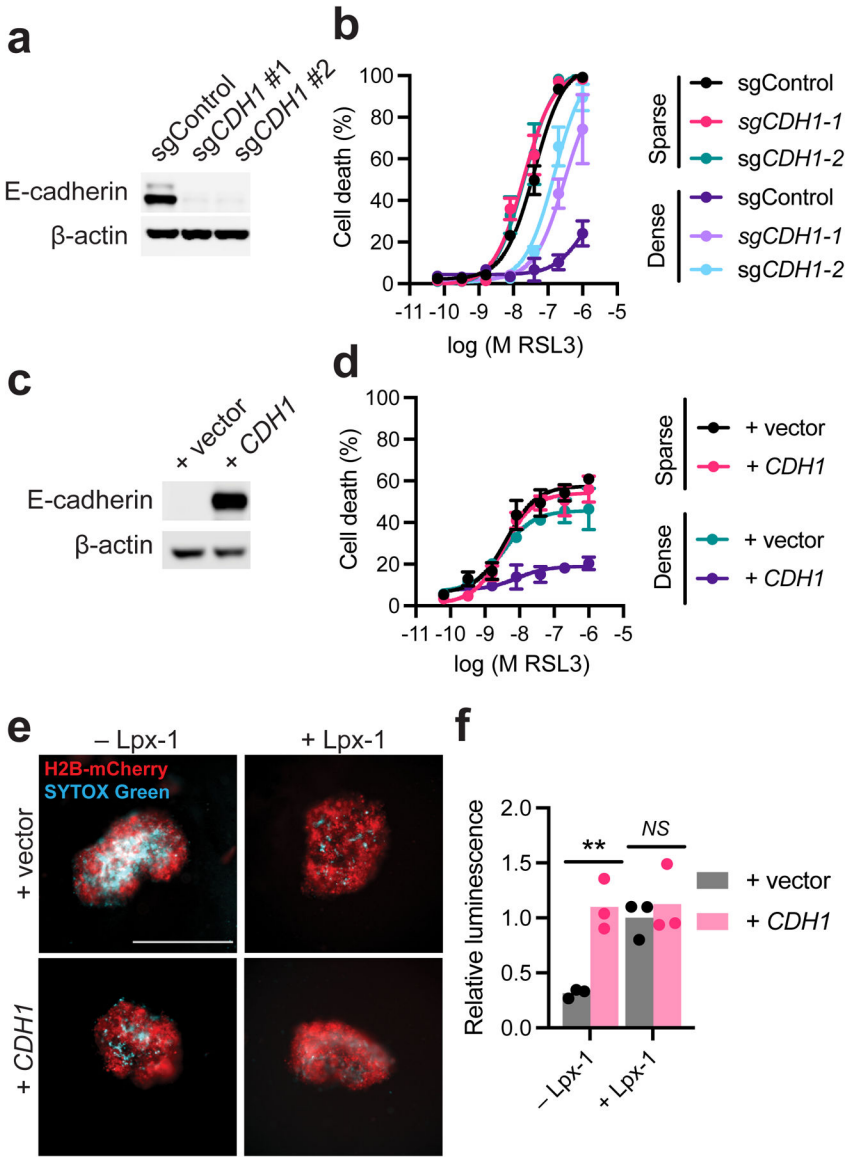

Figure 2. E-cadherin expression dictates cell density-regulated ferroptosis in DGC cells.

a, CRISPR-Cas9-mediated E-cadherin knockouts were confirmed in SNU16 cells by Western blot. **b,** Sparse and dense SNU16 control or sg*CDH1* cells were treated with indicated concentrations of RSL3 for 24 hours. Cell death was measured by Cytation 5 imaging. **c,** Overexpression of E-cadherin was confirmed in SNU668 cells by Western blot. **d,** Sparse and dense SNU668 control or E-cadherin-expressing cells were treated with the indicated concentrations of RSL3 for 24 hours. **e-f,** SNU668 cells expressing a vector control or E-cadherin were cultured into tumor spheroids for 72 hours and treated with 1 μM RSL3 in the presence or absence of 1 μM liproxstatin-1 for an additional 30 hours. Cell death was assessed by SYTOX Green staining (**e**), and viability was assessed by CellTiterGlo (**f**). Statistical analysis was performed by student's t-test. $P = 0.0046$, 0.5756.

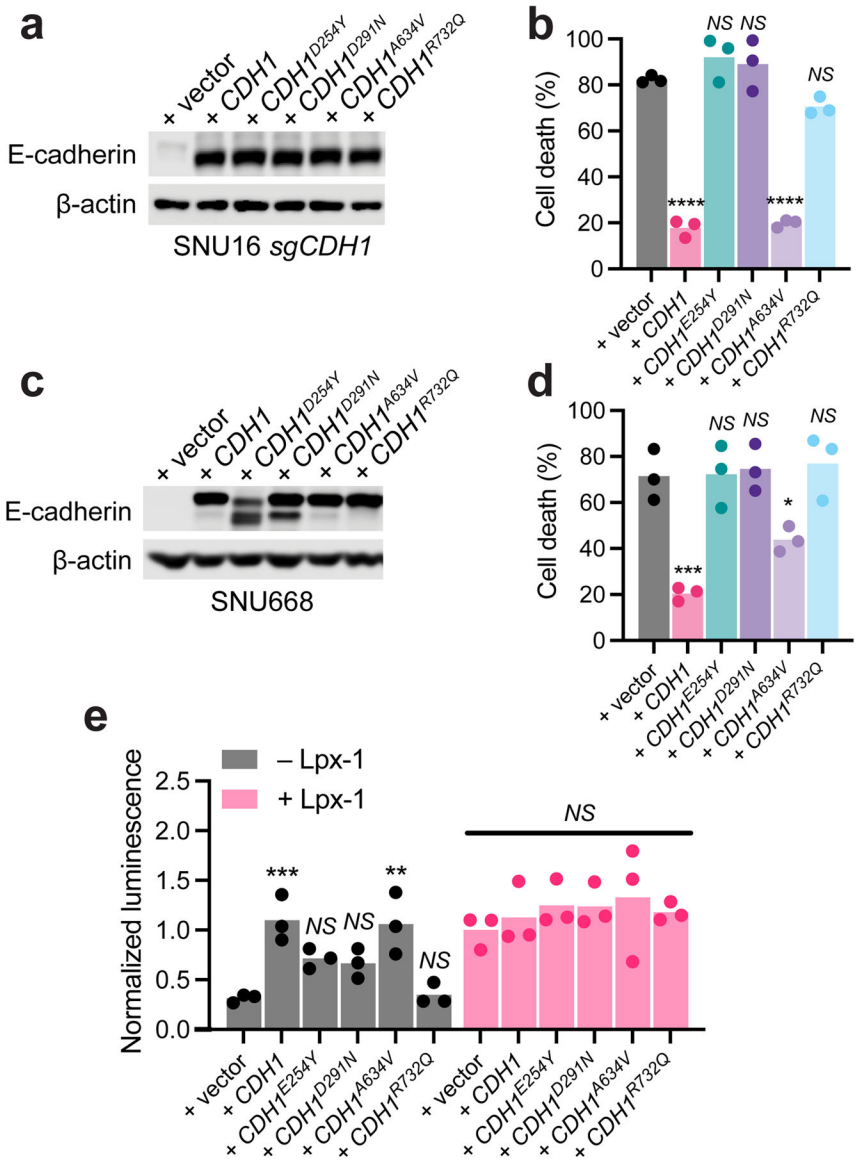

Figure 3. Effect of patient-derived point mutations of E-cadherin on ferroptosis.

a, Expression of the indicated E-cadherin constructs in SNU16 sg*CDH1* cells was confirmed by Western blot. **b,** Dense SNU16 sg*CDH1* cells expressing indicated E-cadherin constructs were treated with 1 μM RSL3 for 24 hours. Cell death was assessed by Cytation 5 imaging. Statistical analysis was performed by one-way ANOVA with Dunnett's multiple comparison test. *P* = < 0.0001, 0.2903, 0.6078, < 0.0001, 0.1560. **c,** Expression of indicated E-cadherin constructs in SNU668 cells was confirmed by Western blot. **d,** Dense SNU668 cells expressing indicated E-cadherin constructs were treated with 1 μM RSL3 for 24 hours. Statistical analysis was performed by one-way ANOVA with Dunnett's multiple comparison test. *P* = 0.0003, 0.9999, 0.9952, 0.0273, 0.9469. **e,** SNU668 cells expressing indicated constructs were cultured into tumor spheroids for 72 hours and treated with 1 μM RSL3 in the presence or absence of 1 μM liproxstatin-1 for an additional 30 hours. Viability was assessed by CellTiterGlo. Statistical analysis was performed by two-way ANOVA with

Šidák's multiple comparison test. $P = 0.0045$, 0.2867, 0.4205, 0.0072, 0.9999, 0.9810, 0.7456, 0.7853, 0.4841, 0.9199.

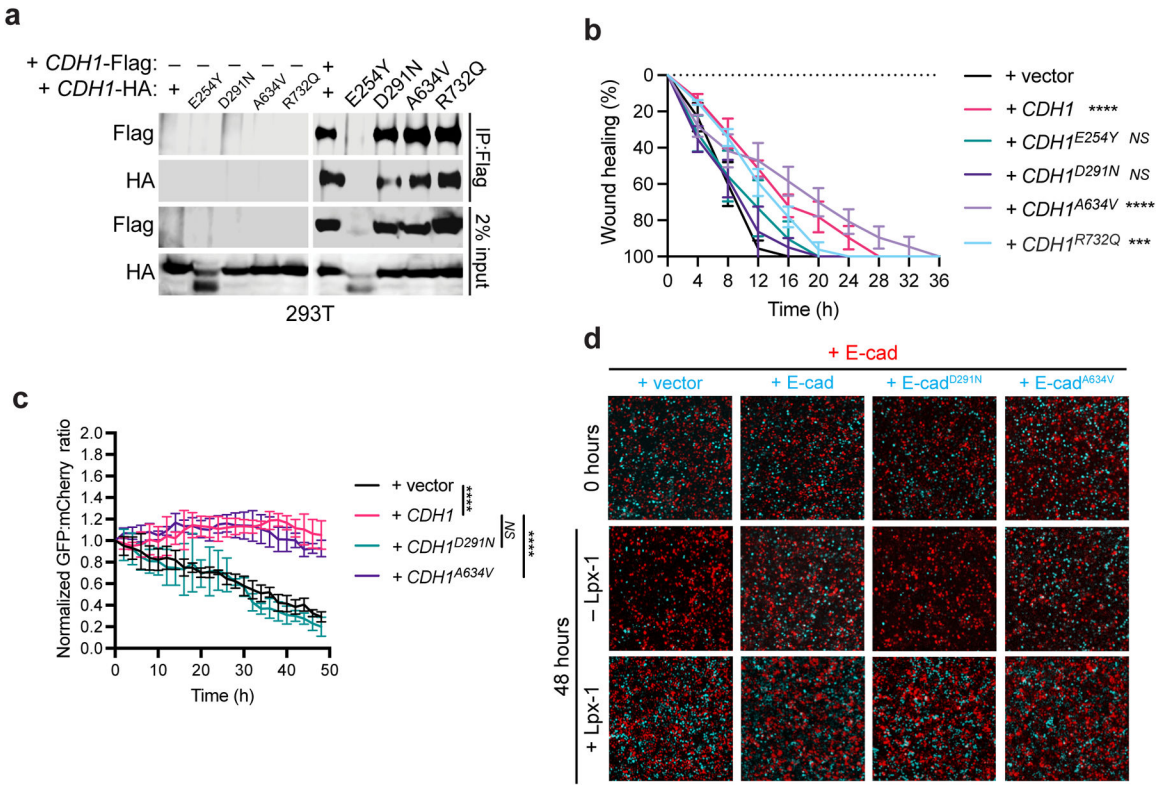

Figure 4. Patient-derived point mutations alters various cellular functions of E-cadherin.

a, 293T cells expressing indicated C-terminal-tagged E-cadherin constructs were co-cultured for 30 hours followed by co-immunoprecipitation for Flag. **b,** Confluent SNU668 cells expressing indicated constructs were subjected to wound healing analysis monitored by Cytation 5 imaging. *P* = < 0.0001, 0.7304, 0.9997, < 0.0001, 0.0014. **c-d,** SNU668 cells expressing indicated constructs and EGFP-tagged H2B were co-cultured with SNU668 cells expressing wild type E-cadherin and H2B-mCherry. Cells were incubated for 30 hours and treated with 1 μM RSL3 in the presence or absence of 1 μM liproxstatin-1. The relative ratio of GFP- to mCherry-tagged cells was monitored over 48 hours by Cytation 5 imaging. *P* = < 0.0001, < 0.0001, 0.7896. All statistical analyses were performed by two-way ANOVA with Dunnett's multiple comparison test.

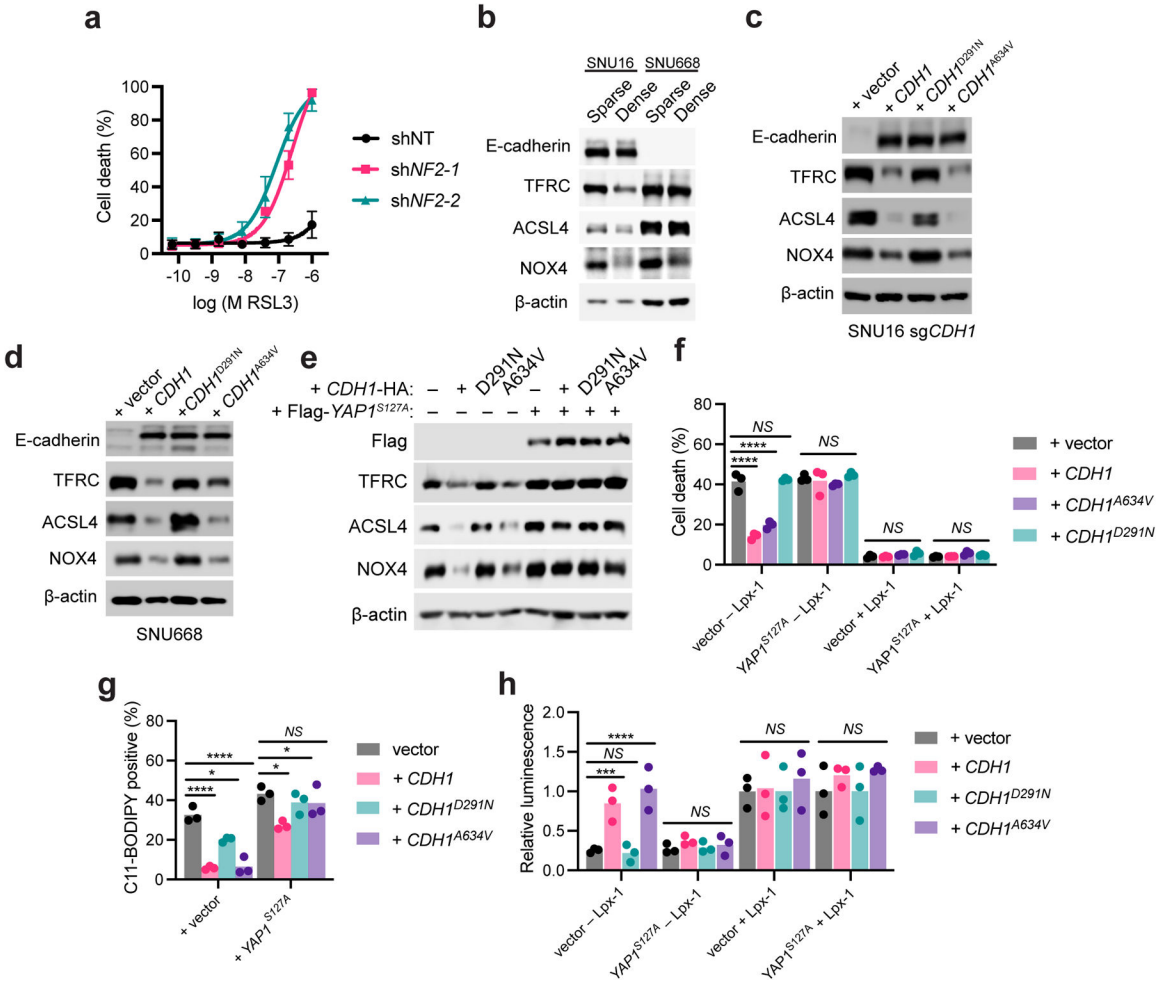

Figure 5. NF2-Hippo-YAP pathway mediates the ferroptosis-regulatory function of E-cadherin in DGC cells.

a, Dense SNU16 cells expressing hairpins targeting a control sequence or *NF2* were treated with various concentrations of RSL3 for 24 hours. Cell death was measured by Cytation 5 imaging. **b-d,** Expression of ferroptosis-related genes regulated by YAP was assessed by Western blot in sparse or dense SNU16 and SNU668 cells (**b**), and SNU16 sg*CDH1* cells (**c**), SNU668 cells (**d**) or SNU668 cell expressing the constitutively active Flag-YAP^{S127A} mutant (**e**) expressing the indicated E-cadherin mutants. **f,** SNU668 cells expressing either a vector control or the constitutively active Flag-YAP^{S127A} mutant were treated with 1 μM RSL3 in the presence or absence of 1 μM liproxstatin-1 for 24 hours. *P* = < 0.0001, 0.9075, < 0.0001, 0.7962, 0.6922, 0.2039, 0.9999, 0.7493, 0.9241, 0.9991, 0.9524, 0.6583. **g,** Indicated cell lines were treated with 0.5 μM RSL3 for 18 hours and stained with C11-BODIPY. Lipid peroxidation was measured by flow cytometry. *P* = < 0.0001, 0.0080, < 0.0001, 0.0010, 0.4788, 0.4177. **h,** Indicated cell lines were cultured into tumor spheroids for 72 hours, treated with 1 μM RSL3 in the presence or absence of 1 μM liproxstatin-1 for 24 hours, and viability was measured by CellTiterGlo. *P* = 0.0072, 0.9957, 0.0005, 0.8994, 0.9991, 0.9835, 0.9936, 0.9999, 0.7143, 0.5478, 0.9999, 0.3135. All statistical analyses were performed by two-way ANOVA with Dunnett's multiple comparison test.

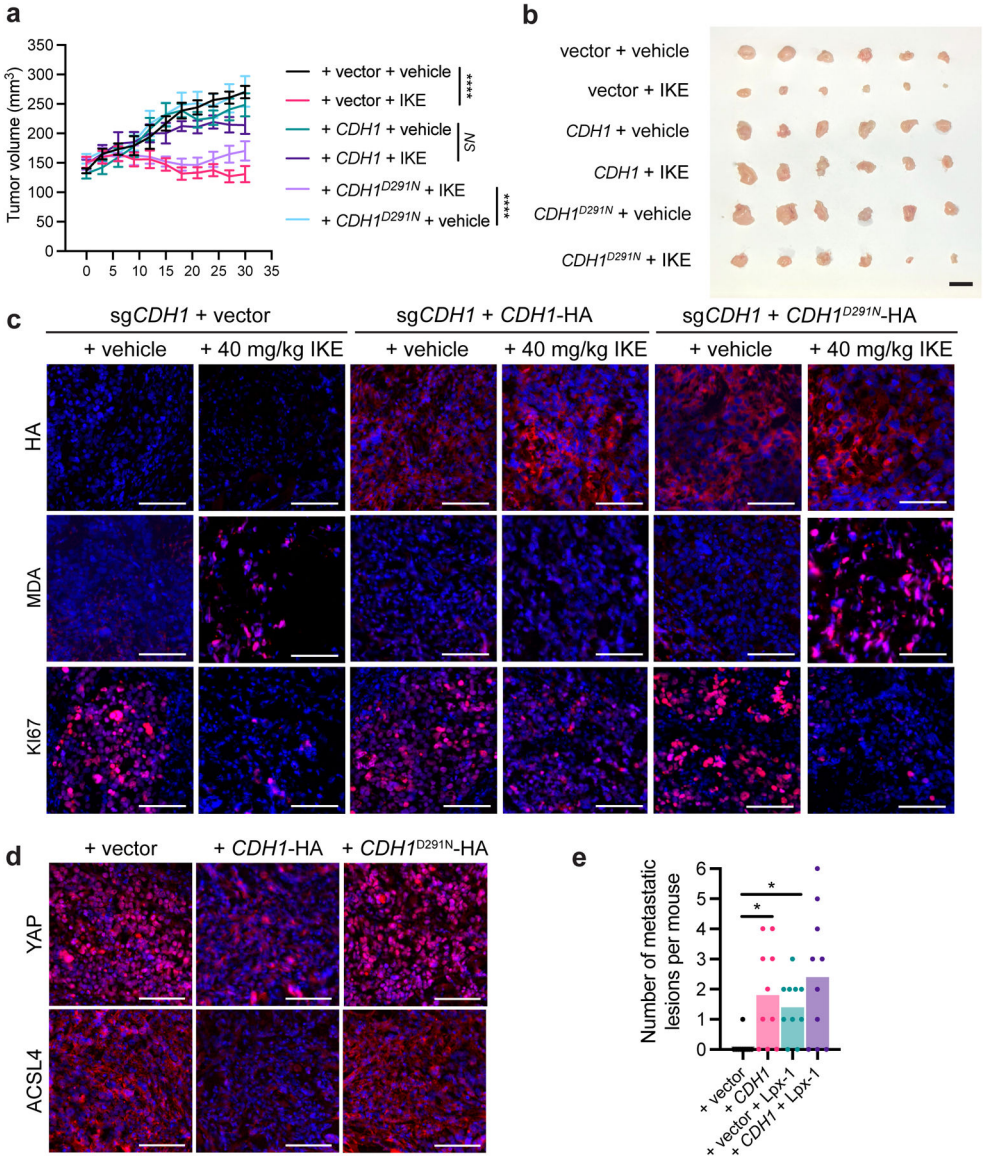

Figure 6. E-cadherin mutation sensitizes DGC cells to ferroptosis induction *in vivo* and mitigates lung metastasis of circulating DGC cells.

a, Subcutaneous SNU16 sg*CDH1* xenografts expressing indicated HA-tagged E-cadherin constructs were monitored every three days by caliper, and tumor volume was recorded. Statistical analysis was performed by two-way ANOVA with Tukey's multiple comparison test. *P* = < 0.0001, 0.8744, < 0.0001. **b,** Excised tumors were briefly washed in PBS and imaged. Scale bar = 1 mm. **c,** Cryosectioned tumors were stained for HA (indicating E-cadherin expression), malondialdehyde (MDA), and Ki67. **d**, Tumor sections were stained for YAP and ACSL4 expression. **e,** SNU16 sg*CDH1* cells expressing iRFP-720 and indicated constructs were injected intravenously into mice. After four weeks, lungs were excised and scanned for clusters of greater than 50 cells expressing iRFP-720. Statistical analysis was performed by Kruskal-Wallis test with Dunn's multiple comparison test. *P* = 0.0102, 0.0184, 0.9999.